Super-Diffraction Longitudinally Polarized Optical Needle With Ultra-Long Focal Depth Generated by a Radially Polarized High-Dimensional Circular Hollow Sinh-Gaussian Beam

Si-Mo Wang , Wei Yan , Fan-Xing Li , Fu-Ping Peng , and Jia-Lin Du

Abstract—In this paper, the incident beam called high-dimensional circular hollow sinh-Gaussian (HD-CHsG) beam with a novel wavefront is proposed, which is determined by three parameters (m, σ_0, σ_1). Based on the Richards-wolf vector diffraction theory, it can be focused into a longitudinal polarized optical needle through a high numerical aperture lens. The effects of the three parameters (m, σ_0, σ_1) on the resolution and depth of focus of the longitudinally polarized optical needle are simulated and analyzed. In the condition of (m, σ_0, σ_1) = (8, 0.6, 0.125), a super-diffraction longitudinal optical needle with ultra-long focal depth (resolution 0.40λ, focal depth 18.36λ, depth-to-width ratio 45.9:1) is generated. In addition, compared with a radially polarized incident beam whose amplitude distribution is Gaussian and circular hollow sinh-Gaussian (CHsG) distribution, the resolution and depth of focus of the longitudinally polarized optical needle obtained by focusing the HD-CHsG beam are higher. Both simulations and experiments are carried out to demonstrate the availability of our method. Our findings are of great significance to the production, manipulation, and application of longitudinally polarized optical needle.

Index Terms—Optical needle, super-diffraction, ultra-long focal depth, vector diffraction theory, high-dimensional circular hollow sinh-gaussian beam.

I. INTRODUCTION

OPTICAL needle with resolution beyond the diffraction limit and ultra-long focal depth play an important role in many applications, such as particle acceleration [1]–[4], optical trapping [5], [6], fluorescent imaging [7], material processing [8], optical data storage [9], and super-resolution microscopy

[10]. The Abbe diffraction resolution limit (0.5λ/NA) indicates that the spatial resolution of the microscope imaging system is directly proportional to the incident beam wavelength (λ), and inversely proportional to the numerical aperture (NA) of the optical system [11]. Using a short-wavelength illuminating beam and a high NA lens can improve the resolution, but it cannot make the resolution exceed the diffraction limit. For one thing, the focus of special electromagnetic wavebands and the scarcity of imaging medium materials limit the reduction of the wavelength of the incident beam. For another thing, the numerical aperture of the focusing objective NA = $\eta \sin \alpha$ (η is the refractive index of the immersion liquid, and α is the maximum half-angle of convergence) can't be increased indefinitely. In addition, the resolution of the focused spot (FWHM = $k_1 \lambda$/NA) is inversely proportional to the depth of focus (DOF = $k_2 \lambda$/NA^2) [12]. Using a short-wavelength incident beam and a high-NA lens to improve the resolution comes at the cost of a shorter focal depth. Therefore, it is challenging to obtain an optical needle with super-diffraction resolution and ultra-long focal depth under the condition of limited wavelength λ and NA.

The appearance of a cylindrical vector beam, especially a radially polarized beam, provides a potential solution to this problem. The optical needle named by Wang *et al.* has attracted wide interest because it satisfies sub-wavelength (0.43λ) and non-diffraction [13]. It is generated by tightly focusing a radially polarized Bessel Gaussian beam modulated by a phase filter. Following the work by Wang *et al.*, various researches have emerged to improve the resolution and DOF of the optical needle. Among these researches, the focus is on optimizing the structure of the filter [13]–[20]. For example, Lin *et al.* designed an amplitude filter through Euler transformation to obtain a longitudinally polarized optical needle with a resolution of 0.8λ and a focal depth of 9λ [14]. Zhan *et al.* generated a high-purity longitudinal polarized optical needle (FWHM = 0.405λ, DOF = 8λ) by discrete complex pupil filter [15]. Using the filter to adjust the amplitude or phase of the incident beam can improve the resolution and focal depth of the optical needle. However, the design of the filter is complicated, the manufacturing is difficult, and the conversion efficiency is low. In addition, the center of the filter needs to be coaxial with the center of the objective lens. Therefore, the method of generating optical needles based

on filter modulation makes some applications more difficult or even impossible.

In recent years, it has been frequently reported that the input beam's wavefront is carefully designed to obtain an optical needle with high resolution and long focal depth. For example, Kitamura *et al.* used a high NA aspheric lens system to focus a radially polarized narrow-width annular Bessel-Gaussian beam to generate a sub-wavelength beam [21]. The FWHM of the focal spot is approximately 0.4λ and the DOF is more than 4λ. Kozawa *et al.* used a higher-order radially polarized Laguerre-Gaussian beam [22]. When the radial mode order p is 12, the lateral resolution is enhanced. Lin *et al.* analyzed the characteristics of the sub-wavelength structure produced by a radially polarized doughnut Gaussian illumination beam [23].

The above studies have shown that the hollow beam can be used to improve the resolution and DOF of the optical needle. The generation, propagation, and focusing characteristics of hollow beams with different amplitude distributions have aroused widespread interest in recent years [24]–[26].

In 2012, Sun *et al.* proposed a generalized hollow sinh-Gaussian (GHsG) beam, which is a new type of Hermite-sinusoidal-Gaussian beam [27]. The circular hollow sinh-Gaussian (CHsG) beam is a general form of the CHSG beam. It is widely used in optical tweezers and optical traps because of its hollow structure characteristics [28]–[30]. In addition, based on the radially polarized CHsG beam, Lin *et al.* obtained a longitudinally polarized spot with a radius of 0.47λ and a high beam quality of 83.4% by selecting the beam order of $m = 8$ [31]. Huang *et al.* studied the radiation force of the CHsG beam acting on Rayleigh metal particles [32]. This method greatly improved the stiffness of the radial trap and expended the distance of the axial trap. Sundaram *et al.* used an azimuthally polarized CHsG beam to obtain an optical needle [33]. A seven-belt complex filter and a spiral phase hologram filter are designed to jointly control the phase and amplitude of the incident beam. However, it is difficult to fabricate and the optical conversion efficiency is low. Moreover, the sidelobe intensity of the obtained optical needle is obvious. Murugesan et.al studied the characteristics of surface plasmon polaritons excited by radially polarized CHsG beam and achieved the lateral and axial confinement in the generated plasmonic focal spot by manipulating the beam parameter (m, ω_0) [34]. However, an optical needle with long focal depth and high resolution cannot be realized. Senthilkumar *et al.* realized a variety of new focal spot patterns by adjusting the beam order m, waist size ω_0, and spirality C of the spirally polarized CHsG beam [35]. Among them, the resolution and focal depth of the optical needle structure obtained in this study are 0.41λ and 2.54λ, respectively. The optical needle structure with a higher aspect ratio is not obtained.

In this paper, based on the research of the CHsG beam, a novel wavefront determined by three parameters (m, σ_0, σ_1) is obtained through the electric field of the GHsG beam, which we named as high-dimensional circular hollow sinh-Gaussian (HD-CHsG) beam. According to the Richards and Wolf vector diffraction theory, the focus characteristics of three radially polarized beams with different amplitude distributions (Gaussian, CHsG, HD-CHsG) are simulated and analyzed. The results

show that the HD-CHsG beam has better focusing performance. After that, the influence of the parameters (m, σ_0, σ_1) on the longitudinally polarized optical needle is also analyzed in detail. In the following, we will use "optical needle" to replace the term "longitudinally polarized optical needle". Under the condition of (m, σ_0, σ_1) = (8, 0.6, 0.125), an optical needle with a resolution of 0.4λ and a DOF of 18.36λ has been obtained. We established an experimental system and indirectly verified the method through the magnifying microscope method. The experimental results show that the transverse optical intensity distribution is highly consistent with the simulation result of the vector diffraction theory. In addition, the DOF of the optical needle measured by the experiment is 16λ, and the measurement error is 13.1%. These simulation and experiment results proved the feasibility and superiority of using radially polarized HD-CHsG beam to generate super-diffraction longitudinally polarized optical needles with ultra-long focal depth.

II. RADIALLY POLARIZED HD-CHsG BEAM AND ITS TIGHT FOCUS MODEL

The tight focus model of the incident radially polarized HD-CHsG beam through a high NA objective lens is shown in Fig. 1. The electric field of the HD-CHsG incident beam at the pupil can be defined as Eq. (1) for a high NA objective lens, where $\sigma_0 = \omega_x/f$ and $\sigma_1 = \omega_y/f$. θ is determined by NA of the objective lens and satisfies $0 \leq \theta \leq \arcsin(NA/n)$. $n = 1.0$ is the refraction index of free space. The characteristics of the HD-CHsG beam are determined by parameters m, σ_0, and σ_1, simultaneously. The related derivation process of Eq. (1) is shown in Appendix A.

$$E_m(\theta) = \sinh^m \left[\sin\theta \left(\frac{\cos^2\theta}{\sigma_0^2} + \frac{\sin^2\theta}{\sigma_1^2} \right)^{1/2} \right]$$
$$\exp\left(-\frac{\sin^2\theta\cos^2\theta}{\sigma_0^2} - \frac{\sin^4\theta}{\sigma_1^2} \right). \tag{1}$$

According to the Richards-Wolf vector diffraction theory, the electric field near the focus of the radially polarized HD-CHsG beam can be expressed as Eq. (2)–(3) [10], [13], [36]. $E_r(r,z)$ and $E_z(r,z)$ represent the transverse and longitudinal electric field near the focus $z = 0$, respectively. The azimuthal electric field is zero everywhere in the diffraction field. In Eqs. (2) and (3), $\alpha = \arcsin(NA/n)$ represents the maximal value of the convergence angle θ, NA is the numerical aperture of the objective lens (NA = 0.95), n is the refractive index of the immersion liquid ($n = 1$), A is the coefficient of power ($A = 1$), $k = 2\pi n/\lambda$ is the wavenumber, J_0 and J_1 denote Bessel functions, and the wavelength $\lambda = 532nm$.

$$E_r(r, z) = A \int_0^\alpha \sqrt{\cos\theta} \sin(2\theta) E_m(\theta) J_1(kr\sin\theta)$$
$$\exp(ikz\cos\theta)d\theta. \tag{2}$$

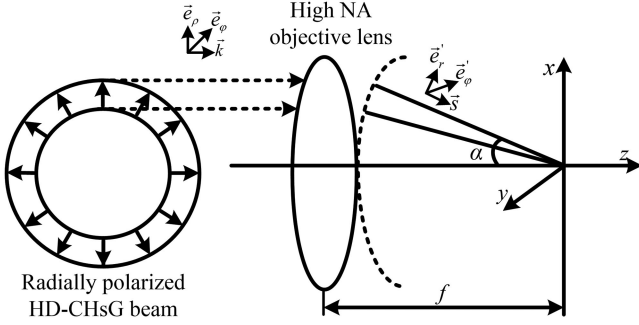$$E_z(r, z) = -2iA \int_0^\alpha \sqrt{\cos\theta}\sin^2\theta E_m(\theta) J_0(kr\sin\theta)$$

Fig. 1. The scheme of the tight focusing system.

$$\exp(ikz\cos\theta)d\theta. \tag{3}$$

Considering that $E_r(r,z)$ and $E_z(r,z)$ are orthogonal, the total electric energy density is given as $I_t = |E_r(r,z)|^2 + |E_z(r,z)|^2$. Some evaluation indicators are used to evaluate optical needles. First, the resolution is characterized by the full width at half-maximum (FWHM) of the optical needle in the radial direction. Second, the depth of focus (DOF) is measured by the axial length whose axial intensity is more than 80% of the maximum axial intensity. Third, the ratio of the maximum value of the longitudinal field over the maximum value of the transverse field is calculated by Eq. (4), which can not only be used to evaluate the specific gravity of the longitudinal field of the optical needle but also can characterize the sidelobe suppression ratio. The obtained super diffraction longitudinally polarized optical needle with ultra-long depth is always expected to have a large sidelobe suppression ratio.

$$M = \frac{I_{z_{\max}}}{I_{r_{\max}}}. \tag{4}$$

III. NUMERICAL SIMULATIONS FOR THE RADIALLY POLARIZED HIGH-ORDER HOLLOW SINH-GAUSSIAN BEAM AND ITS FOCUSING PROPERTIES

A. Numerical Simulation Results and Analysis of the HD-CHsG Beam

Using the expression of the electric field defined by Eq. (1), the intensity distribution of the HD-CHsG beam is determined by the parameters m, σ_0 and σ_1. When m is 2, 4, 6, and 8, the normalized intensity of the HD-CHsG beam with specific $\sigma_0 = 0.6$ and $\sigma_1 = 0.375$ is shown in Fig. 2(a). It is easy to see that the maximum intensity position of the HD-CHsG beam remains unchanged under different m, while the beamwidth decreases as m increases. Obviously, in the case of the same σ_0 and σ_1, the HD-CHsG beam with a larger m focused by a high NA lens has a higher effective NA. In contrast, the intensity distributions of HD-CHsG beams with different parameters σ_0 and σ_1 are also investigated. In the case of $m = 2$, and $\sigma_1 = 0.6$, when σ_0 is 0.125, 0.25, 0.375, and 0.5, the normalized intensity distribution of the HD-CHsG beam is shown in Fig. 2(b). The position of the maximum intensity of the HD-CHsG beam is shifted to the right while the value of σ_0 is increasing. However, as shown in Fig. 2(c), the position of the maximum intensity

of the normalized intensity distribution of the HD-CHsG beam remains unchanged with different σ_1 in the case of $m = 2$ and $\sigma_0 = 0.6$. Contrary to Fig. 2(a), the beam width is proportional to σ_1. The HD-CHsG beam with a smaller σ_1 is provided with a higher effective NA when focused by a high NA lens. Therefore, one can control the intensity distribution of the HD-CHsG beam by choosing m, σ_0, and σ_1 reasonably.

B. Focusing Property of Radially Polarized Beams With Three Different Amplitude Distributions

In order to justify the focusing advantage of the HD-CHsG beam with (m, σ_0, σ_1), the tight focus results of the radially polarized HD-CHsG beam and the other two radially polarized beams with different amplitude distributions are compared and studied.

The intensity distributions of the radially polarized incident beam with three different amplitude distributions (Gaussian, CHsG, and HD-CHsG) near the focal point after being focused by a high NA lens are shown in Fig. 3(a), (b), and (c), respectively. The radially polarized Gaussian, CHsG, and HD-CHsG beams are governed by (0, 0.6, 0.6), (2, 0.6, 0.6), and (2, 0.6, 0.375), respectively. Obviously, the transverse field shows a dark hollow shape while the longitudinal field has a sharp peak profile at the focal plane. Therefore, the transverse field is useless for focusing to form the optical needle, and the sharpness of the optical needle depends on the longitudinal field. The blue and the green solid line in Fig. 3(a4), (b4), (c4) are the normalized intensity distributions of the total field along the longitudinal $z = 0$ and radial $r = 0$ directions under each condition. When the amplitude distribution of the incident beam is Gaussian (Fig. 3(a4)), the FWHM, DOF, and M of the optical needle are 0.50λ, 0.96λ, and 6.75, respectively. As shown in Fig. 3(b4), when the amplitude distribution of the incident beam is CHsG, the FWHM, DOF, and M of the optical needle are 0.46λ, 1.22λ, and 9.56, respectively. Compared with the Gaussian beam, the resolution and DOF of the optical needle obtained by the CHsG beam are increased by 8% and 27.1%, respectively. In the case of the same m, the FWHM, DOF, and M of the optical needle obtained by the HD-CHsG beam are 0.42λ, 2.12λ, and 15.73, respectively. Compared with the CHsG beam, the resolution and DOF of the optical needle are increased by 8.7% and 73.8%, respectively. Compared with the other two incident beams with different amplitude distributions, the HD-CHsG beam has a higher degree of freedom in regulation. In addition, adjusting the parameters of the HD-CHsG beam at the same time can make the FWHM, DOF, and M of the optical needle better.

C. Focusing Property of the Radially Polarized HD-CHsG Beam

In order to further verify the proposed scheme, the tight focus characteristics of the radially polarized HD-CHsG beam with different (m, σ_0, σ_1) are studied. Using the electric field expression of the HD-CHsG beam at the pupil defined by Eq. (1) and the vector diffraction theory, the influence of m, σ_0, and σ_1 on the focused optical needle is simulated and analyzed.
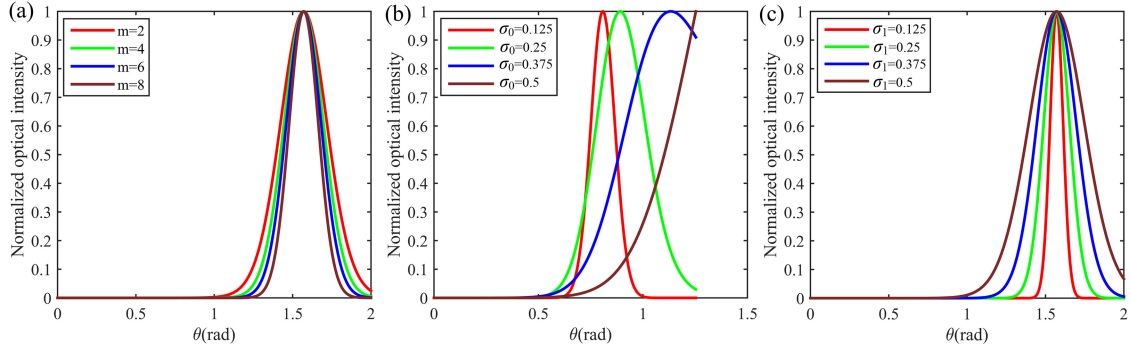
Fig. 2.   Normalized intensity distribution of HD-CHsG beams with different value of parameters (m, σ_0, σ_1) at z = 0. (a) for σ_0=0.6, σ_1=0.375, (b) for m=2, σ_1=0.6, and (c) for m=2, σ_0=0.6.
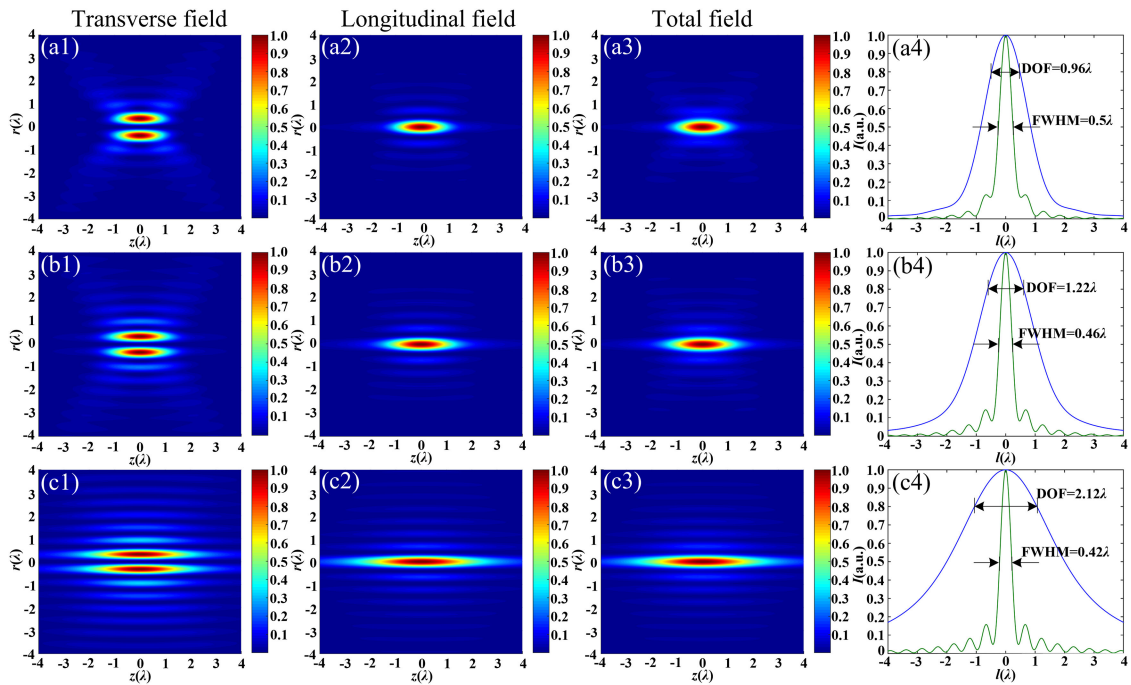

Fig. 3.   Focusing performance of radially polarized beams with three different amplitude distributions with (m, σ_0, σ_1) focused by high NA lens (NA=0.95). (a1)-(a4) for the Gaussian beam with (00.60.6); (b1)-(b4) for the CHsG beam with (20.60.6); (c1)-(c4) for the HD-CHsG beam with (20.60.375). (a1), (b1), and (c1) represent the distributions of the transverse field component. (a2), (b2), and (c2) represent the distribution of the longitudinal field component. (a3), (b3), and (c3) represent the distribution of the total field component. The green and blue solid lines in (a4), (b4), and (c4) represent the normalized intensity distribution of the total intensity of the optical needle in the radial direction (r=0) and longitudinal direction (z=0), respectively.

1) Influence of m on Focusing Spot: In Fig. 4, the simulations of HD-CHsG beam with different m have been presented. In Fig. 4(a4), and (b4), the blue and green solid lines represent the normalized intensity distribution of the focused optical field along the longitudinal ($z = 0$) and transverse ($r = 0$) direction, respectively. When $m = 8$ and $m = 2$, the DOF of the optical needle is 3.60λ and 2.12λ, the former is improved by 69.8% compared with the latter. At the same time, the FWHM of the optical needle is 0.40λ and 0.42λ, the former is 4.8% less than the latter. In the case of the same m, the FWHM of the optical needle changes slightly while the DOF has a significant increase trend as m increases. Therefore, under these circumstances, the

DOF of the optical needle can be increased to a certain extent by increasing m of the HD-CHsG beam.

2) Influence of σ_0 on Focusing Spot: As shown in Fig. 5, for the radially polarized HD-CHsG beam with a specific m and σ_1, we analyzed the influence of σ_0 on the optical needle. As shown in Fig. 5(a1)–(a4), the FWHM and DOF of the optical needle generated by the radially polarized HD-CHsG beam with (2, 0.125, 0.6) are 0.7λ and 2.52λ, respectively. When $\sigma_0 = 0.375$, the FWHM, and DOF of the optical needle are 0.48λ and 1.12λ, respectively. It can be found that the DOF of the focal spot obtained by compressing σ_0 is increased but the resolution is reduced. Therefore, it is impossible to obtain a
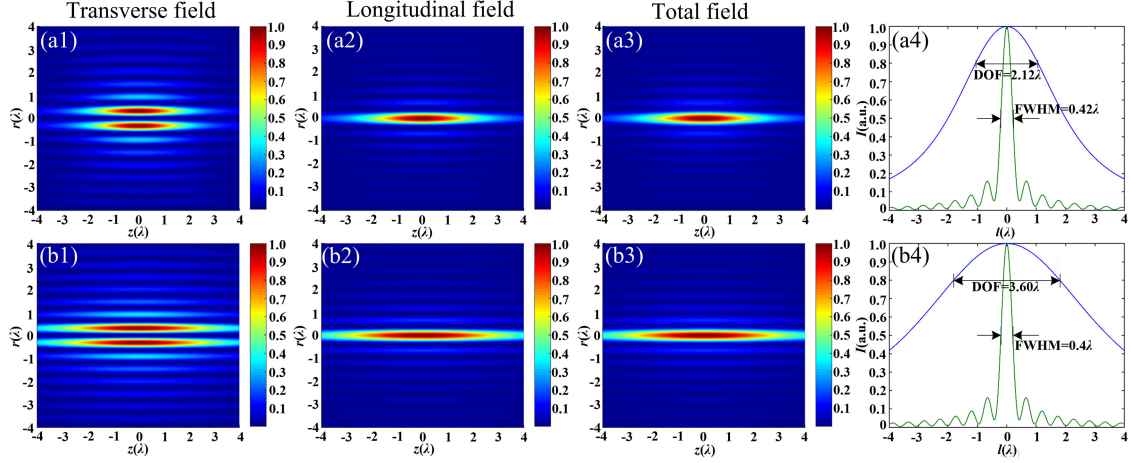
Fig. 4. Focusing performance of radially polarized HD-CHsG beam under different *m* with (*m*, 0.6, 0.375) focused by high NA lens (NA=0.95). (a) and (b) are the optical needles obtained by focusing the HD-CHsG beam when *m* are 2, and 8, respectively. (a1) and (b1) represent the distribution of the transverse field. (a2), and (b2) represent the distribution of the longitudinal field. (a3) and (b3) represent the distribution of the total field. The green and blue solid lines in (a4) and (b4) represent the normalized intensity distribution of the total intensity of the optical needle in the radial direction (*r*=0) and longitudinal direction (*z*=0), respectively.
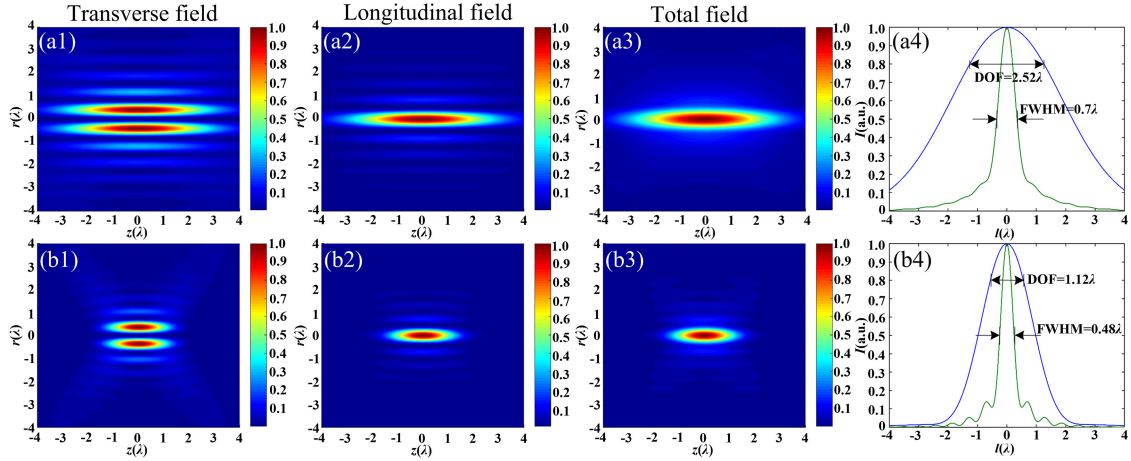

Fig. 5. Focusing performance of radially polarized HD-CHsG beam under different σ_0 with (2, σ_0, 0.6) focused by high NA lens (NA=0.95). (a)-(b) are the optical needles obtained by focusing the HD-CHsG beam when σ_0 are 0.125, and 0.375, respectively. (a1), and (b1) represent the distribution of the transverse field. (a2), and (b2) represent the distribution of the longitudinal field. (a3), and (b3) represent the distribution of the total field. The green and blue solid lines in (a4) and (b4) represent the normalized intensity distribution of the total intensity of the optical needle in the radial direction (*r*=0) and longitudinal direction (*z*=0), respectively.

sharp optical needle structure only by reducing σ_0, mainly because compressing σ_0 will make the transverse field component dominate.

3) Influence of σ1 on Focusing Spot: In addition, under the condition of the radially polarized HD-CHsG beam with specific *m* and σ_0, the influence of σ_1 on the focused optical field is simulated and analyzed as follows. The transverse field, longitudinal field, and total field of the incident HD-CHsG beam with (2, 0.6, 0.125) focused near the focal point through the high NA lens are shown in Fig. 6(a1)–(a3). The FWHM, DOF, and depth-to-width ratio of the optical needle are 0.4λ, 13.6λ, and 34, respectively. As a contrast, under the condition of the radially polarized HD-CHsG beam with (2, 0.6, 0.375), the FWHM, DOF, and depth-to-width ratio of the optical needle are 0.42λ, 2.12λ, and 5.05, respectively. The sidelobe suppression ratio M

of the optical needle in Fig. 6(a3) and (b3) are 25.1489, and 15.73, respectively. Consequently, the longitudinal field of the focused optical field can be increased by compressing σ_1 of the HD-CHsG beam, which is beneficial to improve the resolution and the DOF of the optical needle.

In the above content, not only the focusing performances of the radially polarized beams with three different amplitude distributions (Gaussian, CHsG, HD-CHsG) passing through a high NA lens are investigated, but also the focus characteristics of the HD-CHsG beam with different parameters (*m*, σ_0, σ_1) are studied in detail. The resolution of the optical needle can exceed the diffraction limit, but it is still limited by the super-oscillation criterion. Therefore, the FWHM cannot be less than 0.38λ/NA [37]. In Table I, the resolution, focal depth, depth-to-width ratio, and sidelobe suppression ratio of the
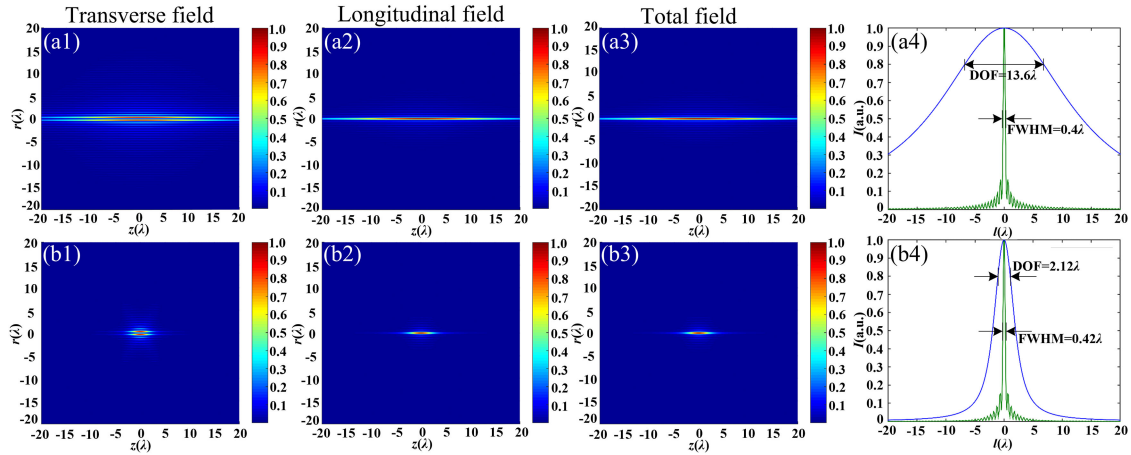
Fig. 6. Focusing performance of radially polarized HD-CHsG beam under different σ_1 with (2, 0.6, σ_1) focused by high NA lens (NA=0.95). (a)-(b) are the optical needles obtained by focusing the HD-CHsG beam when σ_1 are 0.125, and 0.375, respectively. (a1), and (b1) represent the distribution of the transverse field. (a2), and (b2) represent the distribution of the longitudinal field. (a3), and (b3) represent the distribution of the total field. The green and blue solid lines in (a4) and (b4) represent the normalized intensity distribution of the total intensity of the optical needle in the radial direction (r=0) and longitudinal direction (z=0), respectively.

TABLE I
FOCUSING PERFORMANCE OF HD-CHsG BEAM UNDER DIFFERENT
PARAMETERS FOCUSED BY LENS WITH NA=0.95

Rows	(m, σ_0, σ_1)	DOF (λ)	FWHM (λ)	depth-to-width ratio	M
1	(0,0.6,0.6)	0.96	0.50	1.92	6.75
2	(2,0.6,0.6)	1.22	0.46	2.65	9.56
3	(2,0.375,0.6)	1.12	0.48	2.33	7.11
4	(2,0.125,0.6)	2.52	0.70	3.60	3.33
5	(2,0.6,0.375)	2.12	0.42	5.05	15.73
6	(2,0.6,0.125)	13.6	0.40	34	25.1489
7	(8,0.6,0.375)	3.60	0.40	9.00	19.7823
8	(8,0.6,0.125)	18.36	0.40	45.9	25.6988

optical needles with different parameters are compared. From Rows 3 and 4 of Table I, it can be seen that the transverse field of the optical needle is dominant when compressing σ_0. Similarly, as shown in Fig. 7(b), the FWHM and DOF of the optical needle are inversely proportional to σ_0. Therefore, the desired super diffraction longitudinally polarized optical needle with ultra-long depth can't be obtained by a single adjustment of σ_0. On the contrary, the focusing performance can be improved by decreasing σ_1 as shown in Rows 5-6 and Rows 7-8 of Table I. It is obvious from Fig. 7(c) that the FWHM is proportional to σ_1, while DOF is inversely proportional to σ_0. Furthermore, with the same (σ_0, σ_1), the DOF are increased from 13.6λ to 18.36λ in comparison with the value shown in Rows 6 and 8 of Table . It can also be found from Fig. 7(a) that the DOF is proportional to the m, while m has little effect on FWHM. At the same time, comparing Rows 5 and 8 of Table I, the FWHM is reduced to 0.4λ, and the DOF is increased to 18.36λ. The depth-to-width ratio can reach 45.9 in the case of (8, 0.6, 0.125). In conclusion, the focusing performance can be modified with the increase of (m, σ_0) and the decrease of σ_1. It should be noted that here we consider $m = 8$ as a special example to illustrate the focusing advantage of the radially polarized HD-CHsG beam. However, considering the diffraction effect and the limitation

of the amount of light in practical experiments, it is difficult to create the HD-CHsG beam with too large (m, σ_0) and too small σ_1.

IV. EXPERIMENT

A. Experimental Setup

In order to verify our theoretical approach, an experimental setup as shown in Fig. 8 is established. The excitation wavelength of the laser is 532nm. HD-CHsG beams with different parameters can be obtained by modulating the hologram generated by the spatial light modulator. The HD-CHsG beam with (m, σ_0, σ_1) = (8, 0.6, 0.125) is used as the incident beam of the experiment. First, we modified the excitation path of the modified version of the Mach-Zehnder system customized in Refs. [38] and [39]. The transformation of linearly polarized Gaussian beam to radially polarized HD-CHsG beam is achieved by using a spatial light modulator (SLM, X13138 series, HAMAMATSU) and a commercial polarization mode converter (RPC, ECS002180, Arcoptix). Then, a 4f system configured by Fourier lenses L3 and L4 is used to image the SLM plane on the entrance pupil plane of the high NA lens (L5). A spatial filter in the back focal plane of L3 is needed to remove the higher-order diffracted terms generated by the hologram. Finally, the modulated radially polarized HD-CHsG beam is used as the incident beam, which is tightly focused through a high numerical aperture objective lens (NA = 0.95, 100X, Nikon) to generate a longitudinally polarized optical needle.

Since the size of the optical needle is much smaller than the pixel size of the CCD camera, we used a magnification microscope system to capture the focused optical field. The magnification microscope system consists of a 100X objective lens (NA = 0.95, X100, Nikon), a tube lens (f = 200, Nikon), and a CCD camera (resolution of 2048 2048 and pixel size 5.5 μm × 5.5 μm). The objective lens is mounted on a three-dimensional
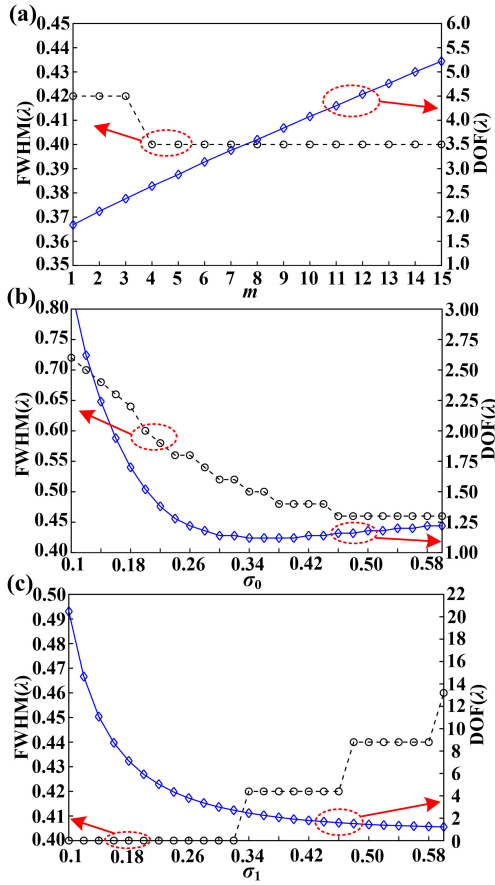
Fig. 7. The relationship between FWHM (blank line) and DOF (blue line) and the parameters m, σ_0, and σ_1, respectively. (a) (m, 0.6, 0.375), (b) (2, σ_0, 0.6), and (c) (2, 0.6, σ_1).
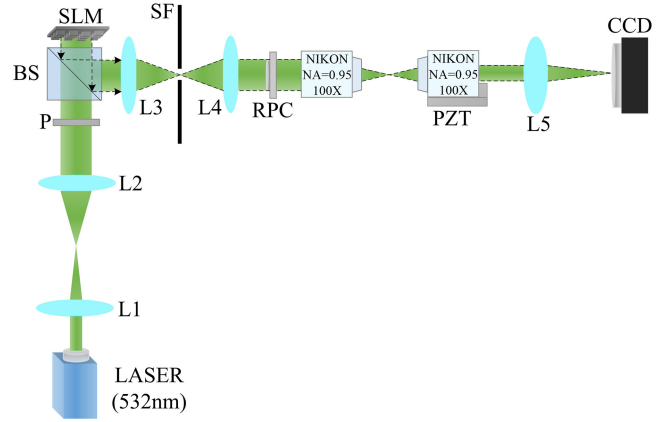

Fig. 8. Experiment setup: L1 and L2 constitute a collimated beam expanding system, P: Polarizer, BS: Beam splitter, SF: spatial filter, RPC: a commercial polarization mode converter, PZT: three-dimensional nano-positioner, L5: tube lens.
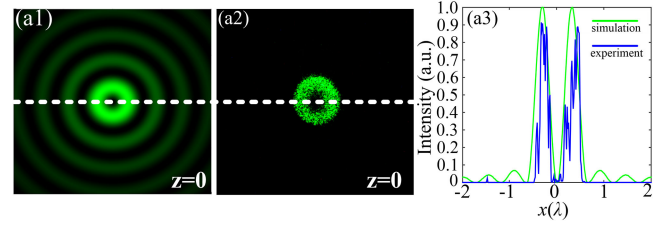

Fig. 9. Transverse optical intensity: (a1) Result of simulation. (a2) Result of the experiment. (a3) The normalized intensity distribution of simulation (solid green line) and experimental (solid blue line) results along the white dashed axis.

nano-positioner (PZT, Micro-Nano Optics) with a linear scanning range of 200 μm and a minimum step length of 1nm.

It is worth noting that the magnifying microscope system not only has the spatial frequency filtering ability but also acts as a polarization filter [40]. Therefore, the longitudinal component of the longitudinal polarized optical needle is always suppressed in the structure of the image. The CCD camera observed is the transverse component of the longitudinally polarized optical needle rather than the total optical field distribution. In this paper, the DOF of the transverse component is measured to indirectly characterize the DOF of the optical needle.

B. Results and Discussion

The simulation and experimental results of the optical field distribution of the transverse component of the optical needle along the radial direction at the focal spot are shown in Fig. 9(a1) and (a2), respectively. Fig. 9(a3) is a comparison diagram of simulation and experimental results along the direction of the white dashed line. It can be seen that the experimental results are in good agreement with the simulation results. The normalized optical intensity of the transverse component obtained by the CCD is basically consistent with the simulation result, which

proves that the resolution of the optical needle obtained by the experiment is consistent with the simulation result.

It is considered that the axial length of the transverse optical field consistent with the simulation result is the DOF of the optical needle measured by the experiment. The intensity distribution of the transverse component of the optical needle captured by the CCD at positions z = -9λ, z = 0, z = 7λ are shown in Fig. 10(a1)–(a3), respectively. Fig. 10(a4) shows the 3D result of the optical field recorded along the z-axis visually. The white bar is equivalent to 0.5λ. The transverse component maintains the intensity distribution similar to the simulation result in the range of z = -9λ to z = 7λ. Therefore, the DOF of the optical needle can be obtained indirectly as 16λ, which is slightly lower than the simulation result. The measurement error is 13.1%.

C. Measurement Error Analysis

It should be noted that in the experiment, problems such as axial deformation and rough edges can be detected in the transverse component field of the optical needle [41], which is mostly produced by the combined impact of the following factors. To begin with, the procedure of using a grating and a 4f filter system to eliminate the SLM's zero-order light cannot entirely eliminate background light, which will influence the
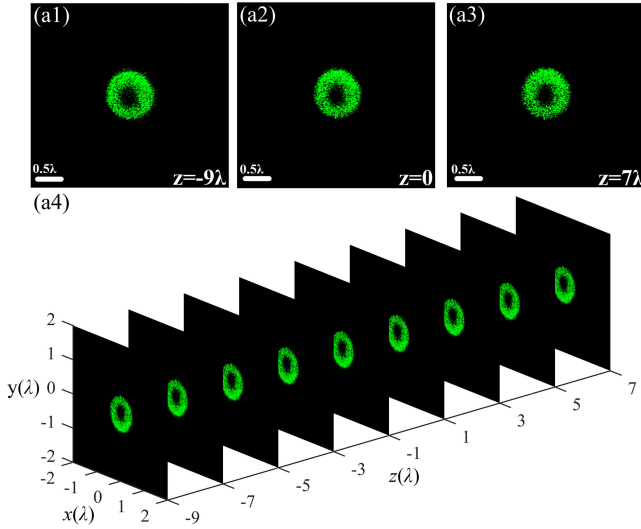
Fig. 10. (a1)–(a3): Experimental results of the irradiance of the imaged field at z = -9λ, z = 0, and z = 7λ, respectively. (a4): Experimental results of the irradiance of the imaging field along the z-axis.

Using the magnifying microscope system, the DOF of the optical needle is indirectly obtained as 16λ, and the measurement error is 13.1%. The experimental results are highly consistent with the theoretical results.

Further study on the lithography exposure methods beyond the diffraction limit will make the three-dimensional characterization of the optical needle possible. Through theoretical and experimental studies, the superiority and feasibility of this method are proved. The super-diffraction longitudinally polarized optical needle with ultra-long focal depth is expected to be widely applied in lithography, optical data storage, and super-resolution imaging.

optical needle observation. Second, the incident beam's homogeneity and stability are crucial influencing elements. Third, the detected transverse optical field component contains axial deformation due to the CCD's limited resolution and pixels, which degrades the profile. Fourth, the stability of the air bearing table, installation error, and the flatness of the optical components will also deteriorate the quality of the transverse component field of the optical needle observed by CCD. Finally, the nano-positioner has stringent operating environment requirements. The drift of the PZT produced by the unstable environment will damage the measurement's precision. Furthermore, it can be found that the side lobes are almost invisible in the experimental results, which is primarily caused by weak sidelobe and insufficient CCD exposure.

V. CONCLUSION

In summary, we proposed a new type of wavefront, which is determined by three parameters (m, σ_0, σ_1). The incident beam with this wavefront is called the HD-CHsG beam. The characteristics of the HD-CHsG beam and its tight focus performances are clarified in this paper. Compared with the radially polarized incident beam with Gaussian distribution and CHsG distribution, the optical needle produced by the HD-CHsG beam has significant advantages. The relationship between the HD-CHsG beam with different parameters (m, σ_0, σ_1) and the characters (FWHM and DOF) of the optical needle is studied. The results show that increasing m and σ_0 while reducing σ_1 can effectively improve the resolution and DOF. Under the condition of (m, σ_0, σ_1) = (8, 0.6, 0.125), a longitudinally polarized optical needle with a resolution of 0.40λ, a focal depth of 18.36λ, and a depth-to-width ratio of 45.9 is obtained. In addition, we demonstrated the generation of the radially polarized HD-CHsG beam with (m, σ_0, σ_1) = (8, 0.6, 0.125) in the experiment, and observed the transverse optical field generated at the focal point.

REFERENCES

[1] S. C. Tidwell, G. H. Kim, and W. D. Kimura, "Efficient radially polarized laser beam generation with a double interferometer," *Appl. Opt.*, vol. 32, no. 27, pp. 5222–5229, 1993.

[2] L. Cicchitelli, H. Hora, and R. Postle, "Longitudinal field components for laser beams in vacuum," *Phys. Rev. A At. Mol. Opt. Phys.*, vol. 41, no. 7, 2008, Art. no. 3727.

[3] J. R. Fontana and R. H. Pantell, "A high-energy, laser accelerator for electrons using the inverse Cherenkov effect," *J. Appl. Phys.*, vol. 54, no. 8, pp. 4285–4288, 1983.

[4] D. Richard, W. Romea, and D. Kimura, "Modeling of inverse Čerenkov laser acceleration with axicon laser-beam focusing," *Phys. Rev. D Part. Fields*, vol. 42, no. 5, pp. 1807–1818, 1990.

[5] Q. Zhan, "Trapping metallic Rayleigh particles with radial polarization," *Opt. Exp.*, vol. 12, no. 15, pp. 3377–3382, 2004.

[6] Q. Zhan, "Trapping metallic Rayleigh particles with radial polarization: Reply to comment," *Opt. Exp.*, vol. 20, no. 6, 2012, Art. no. 6058.

[7] L. Novotny, M. R. Beversluis, K. S. Youngworth, and T. G. Brown, "Longitudinal field modes probed by single molecules," *Phys. Rev. Lett.*, vol. 86, no. 23, pp. 5251–5254, 2001.

[8] M. Meier, V. Romano, and T. Feurer, "Material processing with pulsed radially and azimuthally polarized laser radiation," *Appl. Phys. A*, vol. 86, no. 3, pp. 329–334, 2007.

[9] Y. Zhang and J. Bai, "Improving the recording ability of a near-field optical storage system by higher-order radially polarized beams," *Opt. Exp.*, vol. 17, no. 5, pp. 3698–3706, 2009.

[10] K. S. Youngworth and T. G. Brown, "Focusing of high numerical aperture cylindrical-vector beams," *Opt. Exp.*, vol. 7, pp. 77–87, 2000.

[11] M. Born and E. Wolf, *Principles of Optics, 7th Anniversary Edition.*, Cambridge Univ. Press, 1980.

[12] C. A. Mack, "Resolution and depth of focus in optical lithography," in *Proc. Microlithographic Techniques in IC Fabrication*, vol. 3183, 1997, pp. 14–27.

[13] H. Wang, L. Shi, B. Lukyanchuk, C. Sheppard, and C. T. Chong, "Creation of a needle of longitudinally polarized light in vacuum using binary optics," *Nature Photon.*, vol. 2, no. 8, pp. 501–505, 2008, doi: 10.1038/nphoton.2008.127.

[14] Jie *et al.*, "Achievement of longitudinally polarized focusing with long focal depth by amplitude modulation," *Opt. Lett.*, vol. 36, no. 7, pp. 1185–1187, 2011.

[15] W. Jiming, C. Weibin, and Z. Qiwen, "Engineering of high purity ultra-long optical needle field through reversing the electric dipole array radiation," *Opt. Exp.*, vol. 18, pp. 21965–21972, 2010.

[16] K. Huang, P. Shi, X.-L. Kang, X. Zhang, and Y.-P. Li, "Design of DOE for generating a needle of a strong longitudinally polarized field," *Opt. Lett.*, vol. 35, no. 7, pp. 965–967, 2010.

[17] H. Guo *et al.*, "Tight focusing of a higher-order radially polarized beam transmitting through multi-zone binary phase pupil filters," *Opt. Exp.*, vol. 21, no. 5, pp. 5363–5372, 2013.

[18] Y. Xu, J. Singh, C. J. R. Sheppard, and N. Chen, "Ultra long high resolution beam by multi-zone rotationally symmetrical complex pupil filter," *Opt. Exp.*, vol. 15, no. 10, pp. 6409–6413, 2007.

[19] Y. Zha, J. Wei, H. Wang, and F. Gan, "Creation of an ultra-long depth of focus super-resolution longitudinally polarized beam with a ternary optical element," *J. Opt.*, vol. 15, no. 7, pp. 536–544, 2013.

[20] C. Kuang, X. Hao, X. Liu, T. Wang, and Y. Ku, "Formation of sub-half-wavelength focal spot with ultra long depth of focus," *Opt. Commun.*, vol. 284, no. 7, pp. 1766–1769, 2011.

[21] K. Kitamura, K. Sakai, and S. Noda, "Sub-wavelength focal spot with long depth of focus generated by radially polarized, narrow-width annular beam," *Opt. Exp.*, vol. 18, no. 5, pp. 4518–4525, 2010.

[22] Y. Kozawa and S. Sato, "Numerical analysis of resolution enhancement in laser scanning microscopy using a radially polarized beam," *Opt. Exp.*, vol. 23, pp. 2076–2084, 2015.

[23] J. Lin, R. Chen, H. Yu, P. Jin, M. Cada, and Y. Ma, "Analysis of sub-wavelength focusing generated by radially polarized dough-nut Gaussian beam," *Opt. Laser Technol.*, vol. 64, pp. 242–246, 2014, doi: 10.1016/j.optlastec.2014.05.019.

[24] H. Wang and X. Li, "Propagation of partially coherent controllable dark hollow beams with various symmetries in turbulent atmosphere," *Opt. Lasers Eng.*, vol. 48, no. 1, pp. 48–57, 2010.

[25] C. A. Y., T. E. B. H., and B. B. Y., "Propagation of various dark hollow beams through an optical system in turbulent atmosphere - ScienceDirect," *Opt. Lasers Eng.*, vol. 48, no. 10, pp. 1019–1026, 2010.

[26] Y. Cheng, J. Tong, J. Zhu, J. Liu, S. Hu, and Y. He, "Clad photon sieve for generating localized hollow beams," *Opt. Lasers Eng.*, vol. 77, pp. 18–25, 2016.

[27] Q. Sun, K. Zhou, G. Fang, G. Zhang, Z. Liu, and S. Liu, "Hollow sinh-Gaussian beams and their paraxial properties," *Opt. Exp.*, vol. 20, no. 9, 2012, Art. no. 9682.

[28] K. Prabakaran, V. Karthik, K. B. Rajesh, P. M. Anbarasan, V. Aroulmoji, and A. M. Musthafa, "Focal hole shifting of azimuthally polarized sinh Gaussian beam using cosine phase filter," *Int. J. Adv. Sci. Eng.*, vol. 06, no. 04, pp. 1476–1481, 2020, doi: 10.29294/ijase.6.4.2020.1476-1481.

[29] K. Zhu, R. Liang, Y. Yi, J. Zhu, and H. Tang, "Propagation invariance and dark hollow structures of sinh-Gaussian beams with small complex parameters," in *Proc. J. Phys. Conf. Ser.*, 2021, Art. no. 012163, doi: 10.1088/1742-6596/1732/1/012163.

[30] Z. Liu, X. Wang, and K. Hang, "Enhancement of trapping efficiency by utilizing a hollow sinh-Gaussian beam," *Sci. Rep.*, vol. 9, no. 1, pp. 1–8, 2019, doi: 10.1038/s41598-019-46716-5.

[31] J. Lin, Y. Ma, P. Jin, G. Davies, and J. Tan, "Longitudinal polarized focusing of radially polarized sinh-Gaussian beam," *Opt. Exp.*, vol. 21, no. 11, pp. 13193–13198, 2013.

[32] Z. Zhang, H. F. Xu, J. Qu, and W. Huang, "Radiation forces of highly focused radially polarized hollow sinh-Gaussian beams on a Rayleigh metallic particle," *J. Mod. Opt.*, vol. 62, pp. 754–760, 2015.

[33] C. M. Sundaram, K. Prabakaran, P. M. Anbarasan, K. B. Rajesh, A. M. Musthafa, and V. Aroulmoji, "Tight focusing properties of phase modulated transversely polarized sinh Gaussian beam," *Opt. Quantum Electron.*, vol. 49, no. 1, pp. 1–10, 2017.

[34] R. Murugesan, N. Pasupathy, M. Udhayakumar, K. B. Rajesh, and Z. Jaroszewicz, "Properties of surface plasmon polaritons excited by radially polarized sinh Gaussian beams," *Plasmonics*, vol. 13, no. 2, pp. 419–425, 2018, doi: 10.1007/s11468-017-0526-0.

[35] M. Senthilkumar, K. B. Rajesh, M. Udhayakumar, Z. Jaroszewicz, and G. Mahadevan, "Focusing properties of spirally polarized sinh Gaussian beam," *Opt. Laser Technol.*, vol. 111, pp. 623–628, 2019.

[36] E. Richards and B. Wolf, "Electromagnetic difraction in optical systems. II. Structure of the image feld in an aplanatic system," *Proceedings of the Royal Society of London. Series A. Mathematical and Physical Sciences*, vol. 253, no. 1274, pp. 358–379, 1959.

[37] K. Huang, H. Ye, J. Teng, S. P. Yeo, B. Luk'yanchuk, and C. W. Qiu, "Optimization-free superoscillatory lens using phase and amplitude masks," *Laser Photon. Rev.*, vol. 8, no. 1, pp. 152–157, 2014, doi: 10.1002/lpor.201300123.

[38] D. Maluenda, I. Juvells, R. Martínez-Herrero, and A. Carnicer, "Reconfigurable beams with arbitrary polarization and shape distributions at a given plane," *Opt. Exp.*, vol. 21, no. 5, pp. 5432–5439, 2013.

[39] D. Maluenda, R. Martínez-Herrero, I. Juvells, and A. Carnicer, "Synthesis of highly focused fields with circular polarization at any transverse plane," *Opt. Exp.*, vol. 22, no. 6, pp. 6859–6867, 2014.

[40] T. Grosjean and D. Courjon, "Polarization filtering induced by imaging systems: Effect on image structure," *Phys. Rev. E Statist. Nonlinear Soft Matter Phys.*, vol. 67, no. 4, 2003, Art. no. 46611.

[41] D. Maluenda, I. Juvells, R. Martínez-Herrero, and A. Carnicer, "Modeling axial irradiance distortion in holographic optical needles produced with high numerical aperture lenses," *OSA Contin.*, vol. 2, no. 5, 2019, Art. no. 1539, doi: 10.1364/osac.2.001539.